The Global Conformation of the Hammerhead Ribozyme Determined Using Residual Dipolar Couplings†

Kent Bondensgaard,‡,§,|| Emilia T. Mollova,‡,⊥ and Arthur Pardi*,‡

Department of Chemistry and Biochemistry, University of Colorado, Boulder, Colorado 80309-0215, and Department of Chemistry, University of Southern Denmark, Odense University, DK-5230 Odense M, Denmark

Received December 18, 2001

ABSTRACT: The global structure of the hammerhead ribozyme was determined in the absence of Mg^{2+} by solution NMR experiments. The hammerhead ribozyme motif forms a branched structure consisting of three helical stems connected to a catalytic core. The ^{1}H-^{15}N and ^{1}H-^{13}C residual dipolar couplings were measured in a set of differentially $^{15}N/^{13}C$-labeled ribozymes complexed with an unlabeled noncleavable substrate. The residual dipolar couplings provide orientation information on both the local and the global structure of the molecule. Analysis of the residual dipolar couplings demonstrated that the local structure of the three helical stems in solution is well modeled by an A-form conformation. However, the global structure of the hammerhead in solution in the absence of Mg^{2+} is not consistent with the Y-shaped conformation observed in crystal structures of the hammerhead. The residual dipolar couplings for the helical stems were combined with standard NOE and *J* coupling constant NMR data from the catalytic core. The NOE data show formation of sheared G−A base pairs in domain 2. These NMR data were used to determine the global orientation of the three helical stems in the hammerhead. The hammerhead forms a rather extended structure under these conditions with a large angle between stems I and II (∼153°), a smaller angle between stems II and III (∼100°), and the smallest angle between stems I and III (∼77°). The residual dipolar coupling data also contain information on the dynamics of the molecule and were used here to provide qualitative information on the flexibility of the helical domains in the hammerhead ribozyme−substrate complex.

The hammerhead ribozyme is a small self-cleaving RNA motif that functions in the rolling circle replication mechanism of various plant viroid and satellite RNAs (*1*−*3*). The hammerhead motif consists of 3 stem regions flanking a catalytic core containing 11 conserved nucleotides (Figure 1). Naturally occurring hammerhead RNAs are single molecules that undergo self-cleavage; however, the hammerhead ribozyme motif can be divided into two molecules; one acting as a ribozyme and the other as a substrate (*4*). These *trans*-cleaving systems have been shown to produce site-specific cleavage of RNAs both in vitro and in vivo (*3*, *4*). The hammerhead ribozyme cleaves a phosphodiester bond at a 5′ UH 3′ site (where U is uridine and H is any nucleotide except G), leaving a 2′,3′-cyclic phosphate and a 5′-OH. The cleavage reaction proceeds through a trigonal bipyramid transition state, and full catalytic activity requires divalent metal ions; however, cleavage activity is observed in the absence of divalent ions at very high concentrations of monovalent ions (*3*, *5*, *6*). Because of its small size and its ability to act as a designer RNA restriction enzyme, the hammerhead ribozyme is one of the most studied catalytic RNAs, and a wide variety of biochemical and biophysical techniques have been used to characterize its mechanism and structure [see (*2*, *3*, *7*, *8*) for reviews].

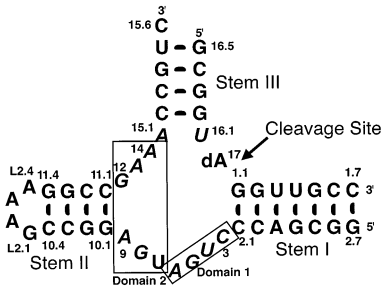

FIGURE 1: Nucleotide sequence and schematic of the secondary structure of the hammerhead construct used in this study. The cleavage site is indicated by an arrow, and domain 1 (residues C3−A6) and domain 2 (residues U7−A9 and G12−A14) are boxed. The 11 conserved residues required for catalytic activity, C3, U4, G5, A6, G8, A9, A12, A13, A14, A15.1, and U16.1, are shown in italics.

Crystal structures have been determined for the hammerhead ribozyme in the presence of Mg^{2+} (*9*, *10*) and absence of Mg^{2+} at high ionic strength (*11*). The hammerhead motif has the same basic structure under these conditions. In the crystals, the hammerhead forms a Y-shaped conformation

† This work was supported by NIH Grant AI 30726, and the NMR instrumentation was purchased with partial support from NIH Grant RR11969 and NSF Grant 9602941. We also thank the W. M. Keck Foundation for support of the Molecular Structure Program on the Boulder Campus.

* To whom correspondence should be addressed. E-mail: arthur.pardi@colorado.edu.

‡ University of Colorado.

§ Odense University.

|| Present address: Health Care Chemistry, Novo Nordisk A/S, Novo Nordisk Park, DK-2760 Måløv, Denmark.

⊥ Present address: Department of Biochemistry, B400 Beckman Center, Stanford University, Stanford, CA 94305-5307.

10.1021/bi012167q CCC: $22.00
Published on Web 09/06/2002

where stem II and stem III coaxially stack to form an extended helix and stem I forms an acute angle with stem II. Unfortunately, the X-ray structures of the hammerhead do not correlate well with the mutational/modification data, and thus the role of the various conserved nucleotides in the cleavage mechanism of the hammerhead is still not well understood (*12, 13*). A possible explanation for this is that the most populated conformation of the hammerhead in the crystals (or in solution) may not be the active conformation. Various conformational changes have been proposed for the hammerhead to proceed from X-ray structure to the catalytically active conformation (*9, 10, 14, 15*), although the extent of these conformational changes is controversial (*16, 17*). A drastically different conformation is proposed for the hammerhead ribozyme in solution in the absence of Mg^{2+}. Fluorescence resonance energy transfer, gel mobility, and transient electric birefringence solution studies indicate that under these conditions, at low ionic strength the hammerhead forms a rather extended conformation (*18*−*20*). Addition of Mg^{2+} triggers the folding of the molecule into the conformation observed in the crystal structures, and this folding has been proposed to occur via a two-step Mg^{2+}-dependent process (*19*). In this paper, we determined the solution conformation of the hammerhead ribozyme in the absence of Mg^{2+}, using residual dipolar coupling data. The global structure under low salt conditions is compared with the crystal structure and with other solution structural models for the hammerhead. The studies here also demonstrate the applicability of recently developed NMR dipolar coupling techniques to the global structure determination of a multidomain RNA.

The dipolar couplings of a macromolecule average to zero in isotropic solution; thus, observation of RDCs[1] requires partial alignment of the molecule (*21, 22*). Unlike local structural parameters such as NOEs and *J* couplings, the RDCs give information on the relative orientation of internuclear vectors in the molecule, and therefore provide long-range structural data. NMR RDCs have recently been used to determine the global domain orientation of multidomain proteins and nucleic acids where the local structures of the domains are known (*23*−*25*). Several approaches have been developed for determining the global structure of multidomain molecules. One method reorients one domain relative to the other by superimposing the PAS of the alignment tensors of the individual domains (*23*). A second method fixes the local structure of the individual domains and then uses rMD calculations to change the relative orientation of these domains to find the best fit to all the RDCs (*26*−*28*). A third method fixes one domain and rotates the other domain as a rigid body, searching for the orientation that provides the best fit to the experimental dipolar coupling data (*24, 25*). We have used the third approach here to determine the global domain orientation of the hammerhead consistent with the NMR data. We found that in the absence of Mg^{2+} the hammerhead ribozyme exists in an extended conformation similar to that predicted from the FRET and gel studies (*18*−*20*). Stems I and II are nearly collinear whereas stem III is oriented with its helical axis almost perpendicular to the other two stems. These studies demonstrate how residual dipolar coupling data can be used to determine the global conformation of RNAs, while also providing qualitative information on the global conformational flexibility for the hammerhead ribozyme.

MATERIALS AND METHODS

Sample Preparation. The 35 nt hammerhead ribozyme (Figure 1) was prepared by in vitro transcription with T7 RNA polymerase using previously described methods (*29*). Nucleotide-specific labeling was achieved by various combinations of uniformly $^{13}C/^{15}N$-labeled and unlabeled NTPs in the transcription mixture. Three different specifically labeled samples were synthesized: a $^{13}C/^{15}N$-adenosine ribozyme, a $^{13}C/^{15}N$-guanosine ribozyme, and a $^{13}C/^{15}N$-uridine/cytosine ribozyme. The RNA transcripts were purified by anion exchange HPLC, and the 3′-end of the transcript was cleaved by a second hammerhead ribozyme to yield a homogeneous 3′-end population, which was further purified by either denaturing PAGE or anion-exchange HPLC (*30*). The noncleavable chemically synthesized 13 nt substrate (Figure 1) was purchased from Dharmacon Research, Inc. (Lafayette, CO), and purified by anion exchange HPLC as described (*30*).

The ribozyme and substrate RNAs were dialyzed extensively against buffer containing 25 mM d_4-succinic acid, pH 5.5, 100 mM NaCl, 0.1 mM EDTA, and 10% D_2O. Substrate was added to the ribozyme to form a 1:1 ribozyme−substrate complex, and the sample was further dialyzed against the same buffer. Before each NMR experiment, the sample was heated to 60 °C for 2 min and cooled on ice to ensure proper complex formation. The concentrations of the NMR samples ranged from 0.6 to 1.9 mM for the complex.

Resonance Assignment. Aromatic ^1H, ^{13}C, and ^{15}N resonances were assigned from 2D (^{15}N, ^1H) and (^{13}C, ^1H) HSQC, (^1H-^1H) NOESY, and base-specific magnetization transfer experiments (*31*−*34*). Intranucleotide H6/H8 to H1′ connections were established from HCN and ^{13}C-edited NOESY experiments (*31*). Ribose ^1H and ^{13}C resonances were assigned from 2D (^{13}C, ^1H) HCCH-COSY and 3D (^1H, ^{13}C, ^1H) and (^{13}C, ^{13}C, ^1H) HCCH-TOCSY experiments (*31*). Sequential assignments were made from ^{13}C-edited NOESY spectra as well as a 3D (^{13}C, ^{13}C, ^1H) HMQC-NOESY-HMQC experiment performed on the uridine/cytosine-labeled sample. All NMR spectra were acquired on Varian Inova 500 or 600 MHz NMR spectrometers operating at 25 °C, using a double- or triple-resonance *z*-axis pulsed-field gradient probe.

Determination of Residual Dipolar Couplings. One-bond ^1H-^{13}C and ^1H-^{15}N RDCs were determined for the $^{13}C/^{15}N$-labeled G, C, and U residues of the ribozyme in the hammerhead ribozyme−substrate complexes. Samples of $^{13}C/^{15}N$-guanosine and $^{13}C/^{15}N$-uridine/cytosine ribozyme−substrate complex were weakly aligned in a medium containing filamentous phage Pf1 (*35*−*37*). The phage was

[1] Abbreviations: CT, constant time; COSY, correlation spectroscopy; DSSE, doublet-separated sensitivity-enhanced spectroscopy; FRET, fluorescence resonance energy transfer; GDO, general degree of order; HCN, proton, carbon, and nitrogen correlation experiment; HCCH, proton, carbon, carbon, hydrogen; HMQC, heteronuclear multiple quantum correlation spectroscopy; HSQC, heteronuclear single quantum correlation spectroscopy; NOESY, nuclear Overhauser effect spectroscopy; NOE, nuclear Overhauser effect; nt, nucleotide; NTP, nucleotide 5′-triphosphate; PAS, principal axis system; RDC, residual dipolar coupling; rMD, restrained molecular dynamics; TEB, transient electric birefringence; TOCSY, total correlation spectroscopy.

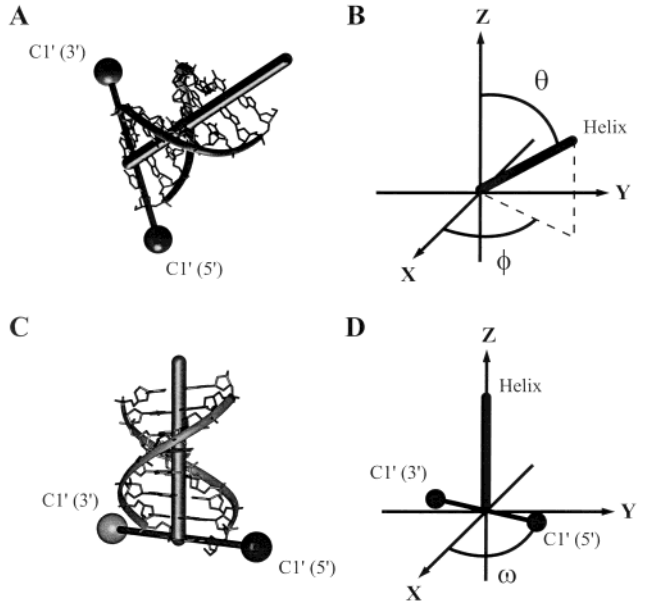

FIGURE 2: Definition of the polar angles used to define the orientations of the helical stems in the hammerhead ribozyme. (A) A helical stem shown with the corresponding helical axis and the vector connecting the two C1′ atoms in the terminal base pair. (B) θ and φ are defined as the polar coordinates of the helical axis in the coordinate frame. (C) The helix from (A) rotated through the polar coordinates θ and φ to position the helical axis along the z axis. (D) ω is defined as the angle between the x axis of the coordinate frame and the projection of the C1′−C1′ vector in the xy plane. The C1′ atom of the 5′-nucleotide defines the head of the C1′−C1′ vector.

dialyzed against 25 mM succinic acid, 100 mM NaCl, 0.1 mM EDTA, and 0.05% NaN_3, pH 5.5, then pelleted by ultracentrifugation and resuspended in the NMR sample buffer twice, and finally added to the RNA sample. The final Pf1 concentrations were ∼15 and ∼30 mg/mL, leading to a deuterium quadrupole splitting for HDO of 16.4 and 28.0 Hz for the uridine/cytosine-labeled and guanosine-labeled samples, respectively.

The one-bond ^{1}H-^{13}C and ^{1}H-^{15}N couplings were measured for samples with and without phage. The ^{1}H-^{15}N couplings were measured from 2D (^{15}N, ^{1}H) t_1-coupled HSQC experiments. A ^{1}H-^{13}C version of the DSSE-HSQC experiment (*38*) was used for measuring the one-bond C8H8 couplings in guanine bases; and a sensitivity-enhanced CT-TROSY experiment (*39*, *40*) was used to measure the one-bond C6H6 and C5H5 couplings in cytidine and uracil bases. The RDCs were calculated from the difference between the couplings measured from the aligned and unaligned spectra. The errors in the measurements were estimated from the difference between dipolar coupling values obtained by manual measurement of peak splittings and values determined through fitting the lines to a Lorentzian curve. These errors range from ±1.0 to 12.0 Hz, with the large errors arising from poorly resolved or broad resonances (see Table S1 of Supporting Information).

The one-bond ^{1}H-^{13}C couplings for ribose CH groups were measured with a *J*-modulated ^{1}H-^{13}C CT-HSQC experiment (*41*). The constant time period was set to $1/J_{CC}$, 25 ms. Ten experiments were acquired for each sample, with a delay, Δ, ranging from 3.8 to 17.0 ms. The couplings were determined by fitting the intensity of the line as a function of Δ, to a cosine function as described (*41*) (see Figure 3B). The errors in these measurements were estimated from fitting, and generally ranged from ±1.0 to 5.0 Hz; however, some couplings had larger errors due to poorly resolved or broad resonances (see Table S1).

Since RDCs were measured for samples with different degrees of alignment (different phage concentrations), a factor of 1.71 was used to correct for differences in phage concentration (∼15 and 30 mg/mL). The factor was calcu-

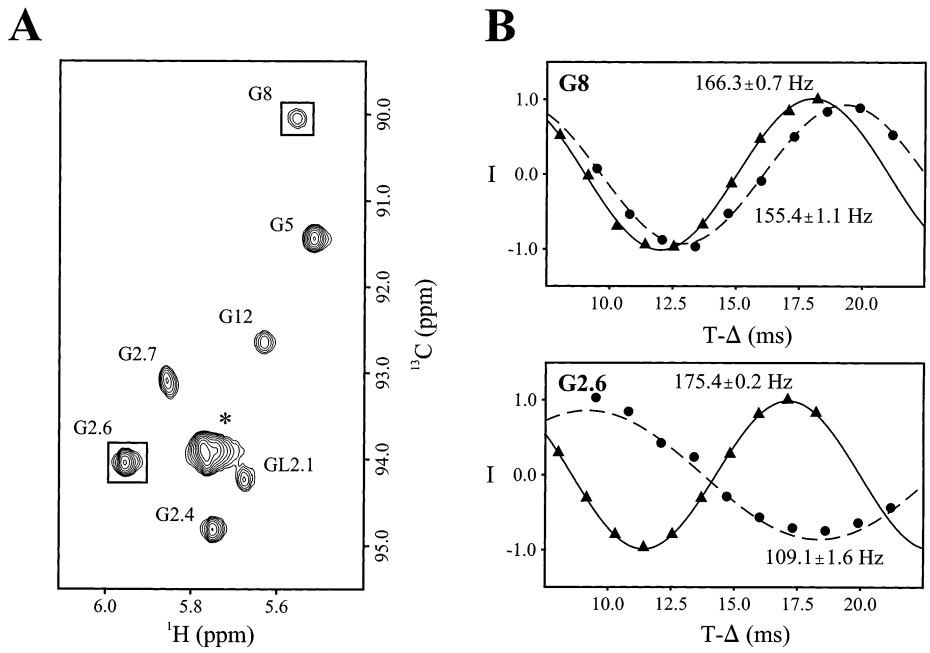

FIGURE 3: (A) The C1′−H1′ region of a *J*-modulated CT-HSQC spectrum of the ^{13}C/^{15}N-guanine-containing sample acquired in isotropic solution, with an evolution time *T*-Δ of 17.1 ms. The asterisk marks the position of the overlapping G10.1, G10.2, G11.3, and G15.4 resonances. (B) A plot of the intensities of the G8 and G2.6 resonances as a function of *T*-Δ in both isotropic (▲) and anisotropic (●) solution. The curves represent the fits of the intensities, measured in isotropic (—) and anisotropic (− −) solution, to the function cos-[$\pi J_{CH}(T\text{-}\Delta)$]. The values of the best fits to the coupling constants are also shown.

lated from the ratio of the splitting of the deuterium line of HOD observed for the two phage concentrations. It has been previously shown that the deuterium splitting is proportional to the phage concentration and to the degree of alignment (*35*).

Determining Global Conformation. The global conformation of the hammerhead ribozyme was determined from residual dipolar coupling data using a modified version of the program Conformist (*24*). The program was adapted to perform simultaneous reorientation of three domains. Since the orientations determined from RDC data are sensitive to variations in local structure, four models for the local structure of each stem were employed. Three of these models were derived from the three copies of the hammerhead ribozyme in the asymmetric unit of the crystal structure by McKay and co-workers [(*9*), PDB identifier 1HMH]. These models are referred to here as: AB, CD, and EF and represent molecules A and B, C and D, and E and F, respectively, in the PDB coordinate file. A fourth model of each stem was generated as a regular A-form double helix with the program InsightII (MSI). The crystal structure by McKay and co-workers consisted of an RNA ribozyme complexed with a DNA substrate (*9*). The RNA:DNA hybrid stems I and III, however, crystallize as A-form helices, and therefore represent a satisfactory model of an all-RNA double helix. The X-ray models were modified to correspond to the sequence of the construct employed here (Figure 1) where: (i) the deoxyribose rings of the substrate strand were changed to ribose rings by adding 2′-hydroxyl groups (except for the cleavage site adenosine dA17); (ii) the cytosine at the cleavage site, dC17, was replaced by dA; (iii) the base pairs U15.5:dA16.5 and dC1.4:G2.5 in the crystal structures were substituted by U15.5:G16.5 and U1.4:G2.4 wobble base pairs, respectively; the atomic coordinates for the G:U base pair in the X-ray structure of a mismatch duplex (*42*) were used for these substitutions; and (iv) thymine bases were replaced with uracil. The three models of the stems based on the crystal structure had an average rmsd of 0.78 Å, while the A-type RNA models differed from the crystal structures by an average rmsd of 1.24 Å.

The global conformation of the hammerhead−substrate complex was described by the set of angles θ, φ, and ω which represent the orientation of each stem relative to stem II. A coordinate frame was chosen in which stem II is oriented with its helical axis along the *z* axis and θ and φ are the polar angles describing the orientation of the helical axis of each stem in this coordinate frame (see Figure 2). The angle ω represents the rotation of the stem about its own helical axis (Figure 2D). To determine ω, the stem was rotated through an angle $-\varphi$ about the *z* axis and then through an angle $-\theta$ about the *y* axis. These rotations position the stem's helical axis parallel to the *z* axis. ω is then determined as the angle between the *x* axis and the projection in the xy plane of the C1′−C1′ internuclear vector of the base pair flanking the core of the ribozyme. The C1′ atom of the 5′-nucleotide in the base pair is considered to be the head of the C1′−C1′ internuclear vector. Coordinates for the helical axes of the stems were calculated with the program CURVES 5.0 (*43*).

Molecular Dynamics Simulations. Molecular dynamics simulations with NOE distance, *J* coupling torsion angle, and RDC restraints were performed on the hammerhead ribozyme−substrate complex using a modified version of XPLOR (*44*) (provided by G. M. Clore, NIH). NOEs were measured from ^{13}C-edited 2D NOESY spectra, and $^3J_{H1'-H2'}$ coupling constants were determined from 3D (^{13}C, ^{13}C, ^{1}H) E-COSY experiments (*45*). Repel NOEs were added for pairs of H1′, H6, and H8 protons in the uridine turn for which no NOEs were observed. All simulations were performed with the AMBER94 force field (*46*) including energy terms for bond lengths, bond and dihedral angles, and nonbonded van der Waals and electrostatic interactions. Tables S1−S4 in the Supporting Information give the constraints used in the structure calculations. Each of the 16 global structures, obtained by stem reorientation with Conformist, was used as input for a separate XPLOR calculation. The torsion angles in the core of the hammerhead ribozyme, including the nucleotide backbone torsion angles (α, β, γ, and ζ), were randomized at the start of the XPLOR calculation, generating five starting structures for each global structure. To maintain the orientation of the stems determined from the calculations with Conformist, simulated RDCs were generated, using an artificial alignment tensor with $A_a = 1.7 \times 10^{-3}$ and $R = 0.55$, and these simulated RDCs were used as constraints. Five simulated RDC restraints per nucleotide were employed in the stems. Rigid body dynamics were employed to keep the local structure of the stems fixed (*42*). The goal of this protocol was to fix the local structure and the relative orientation of the stems while still allowing translation of the stems and rearrangement of the core.

These calculations employed an initial stage of simulated annealing using protocols similar to those previously described (*47*, *48*). For this initial stage, only nucleotides in the core and in the three base pairs flanking the core (C2.1:G1.1, G10.1:C11.1, and C15.2:G16.2) were included in the calculations where the local structure of these three base pairs was fixed. Next the full structures for the three stems were introduced (by superimposition on the base pairs flanking the core) followed by a low-temperature simulated annealing protocol.

During the calculations, the conformation of some of the ribose rings in the core was fixed in either an S- or an N-type conformation (see Table S4) based on the measured $^3J_{H1'-H2'}$ couplings (N-type: $^3J_{H1'-H2'} < 2$ Hz; S-type: $^3J_{H1'-H2'} > 9$ Hz). The distance restraints included 93 NOE restraints for core nucleotides and 120 repel distance restraints between H1′, H6, and H8 protons in the uridine turn (Tables S2 and S3). The NOE distance restraints were assigned qualitatively from peak intensities with an uncertainty of ±0.75 Å. The repel restraints were assigned a lower bound of 5 Å and no upper bound. Four hydrogen bonds for the G8:A13 and A9:G12 base pairs in the purine tract in domain 2 (Figure 1) were enforced with distance restraints between H6−N3 and H2−N7.

RESULTS

Residual Dipolar Couplings in the Hammerhead Ribozyme. The residual dipolar couplings for a partially aligned molecule with a fixed shape can be described by (*21*)

$$D_{PQ} = D_0^{PQ}\boldsymbol{S}A_a[(3\cos^2\theta - 1) + (3/2)R\sin^2\theta\cos(2\phi)] \quad (1)$$

where $D_0^{PQ} = -(1/2\pi)(\mu_o/8\pi^2)h\gamma_P\gamma_Q\langle r_{PQ}^{-3}\rangle$, γ_X is the

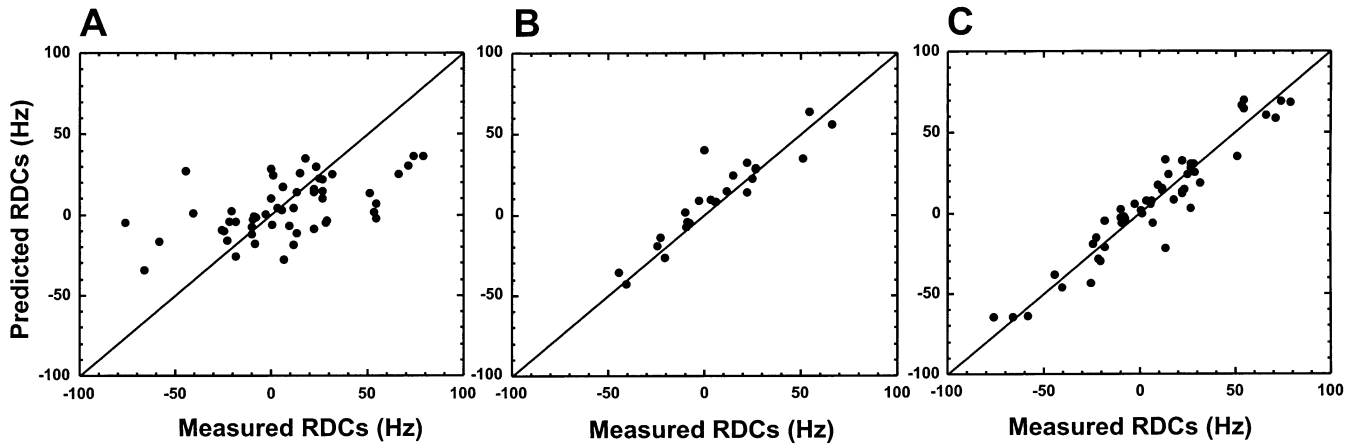

FIGURE 4: Comparison of measured and predicted residual dipolar couplings for the hammerhead ribozyme. (A) All residual dipolar coupling data were fit to the X-ray derived structure model AB. (B) Only data for stem II were fit to the model AB. (C) All data were fit to the solution conformation obtained after domain reorientation.

gyromagnetic ratio of nucleus X, ***S*** is the generalized order parameter, A_{zz}, A_{yy}, and A_{xx} are the principal values of the alignment tensor, $A_a = A_{zz}$ is the axial component of the tensor, R is the rhombicity defined by $R = (2/3)(A_{xx} - A_{yy})/A_{zz}$, and θ and ϕ are the polar coordinates describing the orientation of the internuclear vector r_{PQ} in the PAS of the alignment tensor. In the studies here, ***S*** was assumed to be a constant value for all the residual dipolar couplings. The general degree of order (GDO), which is proportional to the overall degree of alignment of the molecule, was also calculated and is given by (*49*)

$$\mathrm{GDO} = [(2/3)\Sigma_{ij}A_{ij}^{2}]^{1/2} \qquad (2)$$

where A_{ij} represents the components of the alignment tensor.

Partial alignment of the hammerhead ribozyme was achieved using Pf1 phage as a cosolute. These phage have a highly negatively charged surface (p$I \sim 4.0$) and have been previously shown to align negatively charged nucleic acids through steric-type, nonbinding interactions (*35*, *36*). One-bond ^{1}H-^{13}C and ^{1}H-^{15}N RDCs were measured for G, U, and C residues in the various samples of ^{13}C/^{15}N-labeled hammerhead ribozyme−unlabeled substrate complex. Figure 3A shows part of the C1′−H1′ region of the *J*-modulated CT-HSQC spectrum of the guanosine-labeled ribozyme−substrate sample acquired on the isotropic sample. Figure 3B shows the analysis of the *J*-modulated data for two residues in both the oriented and the unoriented samples. The RDCs were only measured for residues on the labeled ribozyme, yielding 27 ^{1}H-^{13}C RDCs for the catalytic core and 62 ^{1}H-^{13}C and ^{1}H-^{15}N dipolar couplings in the stems. Only RDCs from the stems were used in the calculation of the global structure, but the RDCs from the 3′- and 5′-end nucleotides were not included. Thus, 51 RDCs, ranging from −76 to 79 Hz, were used for determining the global conformation of the hammerhead and were distributed as follows: 17 for stem I, 23 for stem II, and 11 for stem III (Table S1).

Comparison between the measured RDCs for these stems and those predicted from the X-ray structure of the hammerhead [structure AB in (*9*)] is shown in Figure 4. The measured RDCs correlate poorly with those predicted from the X-ray crystal structure (Figure 4A). This means that the local and/or global structure of the hammerhead in the crystal differs from that found in solution. However, when the observed and predicted dipolar couplings are compared for each individual stem separately, the correlation improves dramatically (Figure 4B), indicating that the crystal structure is a good representation of the local helical structure in solution. Therefore, significant differences must exist between the global conformation of the hammerhead ribozyme in the crystal and the solution conformation studied here in the absence of Mg^{2+} ions.

Orienting the Stems of the Hammerhead Ribozyme. To obtain the solution conformation of the hammerhead RNA, the relative orientation of the three helical stems was determined from RDC data using the program Conformist (*24*). The program fixes the orientation of one domain in the molecule and then performs a hinge rotation of a second domain (and/or a third domain) relative to the fixed domain. Conformist searches for the global conformation of the molecule that yields the best agreement between experimental and calculated dipolar couplings. Four different sets of atomic coordinates were used in these calculations derived from the three crystal structures and the regular A-type RNA model of the stems (see Materials and Methods). Each of the three helical stems of the hammerhead ribozyme was treated as an independent rigid domain. Domain reorientation was applied to pairs of stems or to all three stems simultaneously. In these calculations, stem II was kept fixed in the molecular frame, and independent hinge rotations were applied to stems I and/or III to generate the set of solution-state conformations. Figure 4C compares the observed and calculated RDCs after the reorientation of the stems for the AB X-ray model, illustrating the good fit of the measured RDCs to the optimized hammerhead conformation.

To assess the consistency of the experimental data for the three stems and the reliability of the results of the stem reorientation procedure, the alignment tensors for each stem and for the entire molecule were calculated with Conformist (Tables 1 and 2). The following sets of RDCs were used: (i) stem II alone; (ii) stems I and II together after reorientation of stem I relative to stem II; (iii) stems III and II together after reorientation of stem III relative to stem II; (iv) all three stems where stems I and III were reoriented relative to stem II. Table 1 presents the results of these calculations for the AB model and shows that the value of the axial component

Table 1: Alignment Tensor Information for Reorientation of Helical Stems in the Hammerhead Ribozyme[a]

stem	II	II− I	II−III	I−II−III
A_a ($\times 10^{-3}$)	1.72	1.65	1.76	1.76
R	0.44	0.37	0.57	0.50
α[b]	300	301	299	300
β[b]	108	107	109	109
γ[b]	111	112	110	111
angle I−II[b]	−	151	−	150
angle III−II[b]	−	−	109	106

[a] The results are for the AB X-ray model and are relative to stem II which was held fixed. Tables S5 and S6 in the Supporting Information give similar results where stems I and III are held fixed, respectively. [b] All values for the angles are in degrees.

Table 2: Components of the Alignment Tensor for the Three Stems of the Hammerhead Ribozyme

	A_a ($\times 10^{-3}$)		R		GDO($\times 10^{-3}$)	
domain	X-ray[a]	A type	X-ray	A type	X-ray	A type
stem I	1.62	1.79	0.21	0.17	1.65	1.81
stem II	1.62	1.73	0.48	0.44	1.76	1.85
stem III	−1.75	−1.65	0.37	0.32	1.84	1.71
full HH[b]	1.71	1.74	0.50	0.47	1.86	1.88

[a] The values of A_{ij} and R for the X-ray structure are averages over the results from the three X-ray-derived model structures AB, CD, and EF (*9*). [b] The values for the whole molecule are calculated after domain reorientation.

of the tensor, A_a, is independent of which stems are reoriented. There are some differences in rhombicity, R, which likely reflect the rather limited set of RDCs in the hammerhead and that R is often difficult to define precisely even with an extensive set of couplings (*50, 51*). Significantly, the Euler angles defining the orientation of the PAS of the tensor (relative to the molecular frame for stem II) are essentially the same. Thus, the components and Euler angles of the tensor are unchanged no matter which set of RDCs are included in the stem reorientation with the program Conformist. The results in Table 1, therefore, indicate that the hammerhead is aligning as a rigid species (*20, 21*) (also see Discussion). Furthermore, the relative orientation of the stems is unchanged independent of whether two or three domains are reoriented (Table 1). Similar results are obtained when stems I or III are held fixed instead of stem II (see Tables S5 and S6 in Supporting Information). This means that the global conformation of the molecule is reliably defined by the experimental dipolar coupling data.

Due to the invariance of a dipolar coupling value with respect to rotation of the domain by 180° about the *x*, *y*, or *z* axes of the alignment frame, there is a 4-fold degeneracy for orienting one domain relative to a second domain (*52*). Because the hammerhead ribozyme has 3 separate domains, this leads to 16 different solution conformations, and Conformist generates all 16 solutions. All these solutions fit equally to the experimental dipolar coupling data; thus, additional information is required to resolve the degeneracy. One solution to this problem involves measuring RDCs in two *independent* alignment media (*53, 54*), but this approach only works if different mechanisms govern the alignment of the molecule in the two media. In our experience with several types of phage as well as a nonionic liquid-crystalline medium (*55*), nucleic acids align by a steric-type mechanism, and no new useful information is obtained when measuring dipolar couplings in these different, but not independent, media (unpublished results). Thus, here we used additional structural information from NOEs, $^3J_{H1'-H2'}$ coupling constants, and the covalent structure to identify the correct solution conformation of the ribozyme among the 16 possibilities.

The arrangement of the stems of the hammerhead in the 16 possible solution structures requires the core of the molecule to adopt conformations very different from the one in the crystal structure. For each of these 16 structures, we tested the ability of the core of the hammerhead ribozyme to accommodate both the new orientation of the stems and the available experimental distance and torsion angle restraints. Cross-strand NOEs for domain 2 in the hammerhead [A9:H2−A13:H1′(strong), A9:H2−G12:H1′(medium), A13:H2−A9:H1′(strong), and A13:H2−G8:H1′(medium)] provided evidence for formation of the two G:A mismatch base pairs, G8:A13 and G12:A9. For domain 1, which forms a uridine turn in the X-ray structures, NOE patterns similar to A-type RNA were observed, and no long-range NOEs expected for a uridine turn were observed. These findings impose additional limitations on the possible conformations of the ribozyme core. Molecular dynamics simulations were used to determine which of the 16 global conformations from Conformist was consistent with the experimental NMR data and the covalent structure of the molecule (see Materials and Methods for details).

Most of the 16 input structures produced a variety of violations predominantly in the regions connecting the core and the stems. In eight of the structures, stems I and II are oriented almost parallel to each other, forcing the connecting nucleotides C4 through A9 to make an extremely sharp turn inconsistent with the observed NOE data. Thus, these solutions for the global structure were discarded. In the remaining eight structures, stems I and II are antiparallel, with a ~150° angle between their helical axes. However, in five of the structures, C11.1 and C15.2 are on the opposite sides of stem II. Thus, it is not possible to satisfy the observed NOEs and also have the purine track G12−A15.1 connect stems II and III without creating steric interference with the reminder of the core. These structures were not considered further.

In two of the remaining three structures, it is possible to connect the stems with the core and still satisfy the NOE restraints. However, to avoid steric clash between stem III and residues 3−5, the uridine turn is forced to adopt a bend which creates steric interference between the backbones (with phosphate−phosphate contacts <6 Å), and these structures were judged not feasible. Only the final structure is free of any NOE and coupling constant violations and had no steric problems. This structure is shown in Figure 5A and represents the global structure of the hammerhead ribozyme in solution in the absence of divalent ions.

To test the role of repel and ^3J coupling restraints on the results, two sets of additional test calculations were performed for the last eight structures; one with the repel distance restraints left out of the restraint list and another set where no restraints were included for the ribose rings in the core. The simulation protocol was identical to that described under Materials and Methods. The resulting structures were not significantly different from those obtained with the full restraint set (see Table S7 in the Supporting

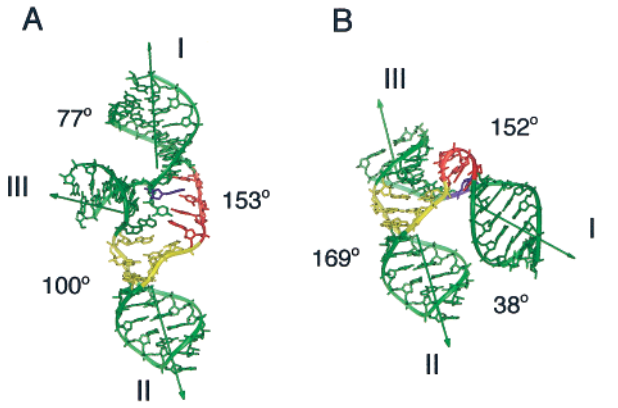

FIGURE 5: Three-dimensional conformation of the hammerhead ribozyme. The interstem angles are shown. (A) Solution conformation derived from dipolar coupling data in the absence of Mg^{2+}. (B) X-ray structure in the presence of Mg^{2+} (*9*).

Information). Thus, the structures mostly depend on structural constraints from the RDCs, the observed NOEs, and the covalent structure.

DISCUSSION

Theoretical Considerations When Applying the Domain Orientation Method to Multidomain Systems. For a multidomain molecule, RDCs contain information on whether the molecule aligns as a single rigid unit in the alignment medium or whether the domains orient independently (*22*−*24*, *49*, *56*). For a rigid multidomain system, the overall ordering of the molecule can be described by a single alignment tensor, and each of the individual domains will have identical alignment tensor components, A_a and R. However, for domains connected by highly flexible linkers, both the magnitudes and the orientations of the alignment tensor will generally be different for the individual domains (*56*).

If the magnitudes of the alignment tensor components are similar in the various domains, this is a strong indication that the molecule is aligning as a relatively rigid species and that RDCs can be used to refine the global structure. However, if the various domains do not have fixed orientations, interdomain motion can lead to an additional averaging of the RDCs for the mobile domain. Tolman et al. (*56*) have recently used simulations to show that an accurate average global conformation of the molecule can still be obtained in the presence of moderate internal motion. However, they found that for large-amplitude motions (>30°) the global structure determined from RDCs deviates from the correct structure.

The general degree of order, GDO, has been used to estimate the effect of internal motions on structure determinations employing RDCs (*49*). To detect the presence of large interstem motions, the alignment tensor and GDO were calculated for each of the helical stems using the RDCs for that stem, and the four different helical models of each stem (see Materials and Methods). The results for the three stems are compared in Table 2 which gives the range of A_a, R, and GDO for the average of the three X-ray models and for the A-form model. To estimate the uncertainty in these parameters arising from both variations in the local structure and errors in the measured RDCs, test calculations were performed using the different helical models and sets of simulated dipolar couplings that mimic the errors in the experimental data. This analysis yielded uncertainties in A_a for the three stems of less than 10%, with most of the variation arising from differences in the local structure.

As seen in Table 2, the magnitudes of A_a and the GDOs for the three stems are very similar, indicating that the stems experience a similar degree of alignment. In particular, the absolute values of the axial components are identical within the error for the three stems. The good agreement between these parameters for stems I and II indicates that the alignment of these two stems can be described by a common tensor, and interstem motion, if present, must be limited. As explained under Results, the somewhat larger difference in the rhombicity R for the stems is most likely a result of the limited set of RDCs available for each stem. Given the similarity between the A_a and the GDOs for stems I and II, the measured RDCs can be directly used to determine the relative orientation of these two stems. However, the results for stem III are more complicated. Although the GDO is similar to that of the other two stems, indicating that stem III experiences the same degree of alignment, A_a for this stem has an opposite sign compared to stems I and II.

The sign of A_a (A_{zz}) contains information on the orientation of the associated principal z axis of the alignment tensor relative to the magnetic field (*57*). For systems with the z axis parallel to the magnetic field, A_a will be positive, and when the axis is perpendicular to the magnetic field, then A_a is negative. For the Pf1 phage system, the alignment of nucleic acids is thought to occur by a steric-type mechanism and depends on the shape of the molecule (*35*, *36*). We have recently measured residual dipolar couplings on tRNA and DNA in several different phage as well as a nonionic (uncharged) liquid-crystalline medium (*55*), and found the same alignment tensor independent of the medium (P. Hanson, A. Vermeulen, and A. Pardi, unpublished results). This provides further confirmation for alignment by a steric-type mechanism where the shape of the molecule dictates the alignment of the nucleic acid. For an elongated shape, the long axis of the molecule (corresponding to the z axis of PAS) should align roughly parallel to the Pf1 phage, which also aligns parallel to the magnetic field, giving a positive sign for A_a. A negative sign for A_a would mean that the long axis of the molecule is no longer parallel to the long axis of the Pf1 phage (the angle must be greater than the magic angle of 54.7°). However, this would be inconsistent with the steric-type alignment mechanism that has been observed for negatively charged Pf1 phage aligning negatively charged nucleic acids (*35*, *36*). Thus, we next consider other mechanisms that could lead to a negative sign of A_a for stem III compared to stems I and II.

There are two other factors that can affect the magnitude or the sign of the components of the alignment tensor of a molecule aligning by a steric-type mechanism. One is the presence of internal motion, and the second is inaccuracies in the experimental data and/or local domain structure. If stem III is only loosely connected to the rest of the hammerhead and hence does not experience significant restriction on its mobility, it could interact with the aligning medium somewhat independent of the rest of the hammerhead. However, steric-type alignment of stem III alone would lead to a smaller GDO for this domain due to the smaller more globular shape of stem III compared to the rest of the

hammerhead, and this is not observed in the hammerhead (Table 2) (*56*). Thus, the change in sign with no change in GDO for stem III compared with stems I and II cannot arise from internal motion when alignment occurs by a steric-type mechanism.

Data inaccuracies or imprecision can also lead to an apparent change in sign of A_a, particularly in cases of limited RDC data. Very small variations in the structure or the RDCs can cause a change in sign in systems with a large rhombicity ($R \approx 2/3$) (*23*). In such systems, the two largest components of the alignment tensor, A_{zz} and A_{yy}, which by definition are of opposite sign, are similar in magnitude. Data variations can cause the magnitude of A_{yy} to become slightly larger than that of A_{zz}, inducing a switch in the principal axes with a concurrent change in the sign of A_a (by definition the *z* axis corresponds to the tensor component with the largest absolute value). However, this requires an *R* close to its maximum value of 2/3, which is not observed for stem III in the hammerhead (Table 2). Nevertheless, examination of the orientation of the axes of PAS for stem II and stem III reveals that a switch of the *z* and *y* axes has indeed occurred for stem III (data not shown). It should be noted that with only 11 RDCs measured for stem III it is expected that the alignment tensor for this stem will be the least accurately defined, and inaccuracy or imprecision for either the RDCs or the local structural model for this stem will have the largest effect on the calculated alignment tensor. To investigate this, stem III was refined with dipolar coupling restraints using the A_a and *R* values determined for stem II. The resulting structure, which satisfied all dipolar couplings, displayed an average change of 8° in the bond vector orientations. In addition, simulations mimicking inaccuracies in the model structures showed that there was a sign inversion when a random change of 8° was applied to the bond vectors. These results suggest that very small differences between the local structure in solution and in the crystal or A-form models for the helical stems in the hammerhead could lead to the observed change of sign.

Thus, the most likely explanation for the observed change in sign of A_a for stem III is the smaller number of experimental RDCs for this stem, combined with some imprecision in the local structural model or the measured couplings. The similar GDOs for all three stems (Table 2) provide strong evidence that the hammerhead is orienting as a single rigid species in solution and that no significant interstem motion is present.

Dynamics of the Global Conformation of the Hammerhead Domain. In addition to providing information on the global structure of multidomain molecules, RDCs also contain information on the dynamics of the molecules. The GDO parameter, which quantifies the degree of alignment of individual domains in a macromolecule, has similar values for all three helical stems in the hammerhead, as seen in Table 2. This is consistent with all three domains in the hammerhead aligning as a single unit and, as discussed above, means that none of the helical domains are undergoing large-scale motional averaging independent of the other two helices. Hagerman and co-workers (*20*) showed that in the absence of Mg^{2+}, the hammerhead RNA with extended arms for stems I and II has essentially the same gel mobility and the same TEB decays as an RNA duplex with length equal to the sum of both extended stems. This means that on the time scale of the TEB experiment ($\sim 10^{-6}$ s) the average conformation and dynamics are similar to those of the linear RNA duplex. Thus, any internal motion changing the relative orientation of the stems must be on a shorter time scale.

Table 3: Relative Stem Orientation for the Hammerhead Ribozyme[a]

domain	angle	NMR[b]	X-ray[c]	FRET[d]
stem I	θ[e]	153 ± 3	38 ± 10	180
	φ	328 ± 4	228 ± 26	N/A
	ω	102 ± 4	181 ± 8	N/A
stem III	θ	100 ± 6	169 ± 9	90
	φ	50 ± 7	45 ± 20	N/A
	ω	286 ± 11	294 ± 41	N/A

[a] All angles are measured in degrees. [b] Values for the global structure calculated from NMR dipolar coupling data, averaged for the X-ray-derived model structures (*9*). [c] Averaged values for the three copies of the molecule in the crystal structure (*9*). The uncertainty is calculated from the dispersion of the values for the three copies. [d] Estimated values from the FRET model in the absence of Mg^{2+} (*19*). [e] The definition of the angles θ, φ, and ω is presented under Materials and Methods.

There are solution data indicating motions in the core of the hammerhead that occur at a much longer time scale. For example, temperature-jump relaxation experiments using 2-aminopurine fluorescence as a probe of conformational dynamics have shown conformational changes in the catalytic core of the hammerhead with lifetimes ranging from a few microseconds to 0.2 s (*58*). Recent ^{19}F NMR studies of the hammerhead also showed exchange-broadening of ^{19}F resonances for 5-fluorouridine substitutions at position U4 or U7 in the catalytic core of the hammerhead (*59*). The ^{19}F NMR data suggest that these residues are experiencing multiple conformations, with exchange lifetimes in the $\sim$1 ms range. We have also measured the power dependence of $T_{1\rho}$ for ^{13}C resonances (*60*) in the hammerhead in the absence of Mg^{2+} (S. A. McCallum and A. Pardi, unpublished results), and these data show evidence for exchange lifetimes in the 10−50 μs range for multiple residues in the catalytic core. This is similar to what was previously reported in the catalytic core of the leadzyme (*61*). Together these results demonstrate that there is significant conformational flexibility in the catalytic core of the hammerhead. However, the residual dipolar coupling data do not show evidence of differential dynamics for any global structural rearrangements of the helical domains in this RNA. Further studies are needed to determine to what extent the local structural dynamics in the catalytic core are coupled to the dynamics for global rearrangement of the helical regions in the hammerhead ribozyme.

Global Conformation of the Hammerhead Ribozyme in Solution. As seen in Figure 5A, the solution conformation of the hammerhead ribozyme determined here in the absence of Mg^{2+} is rather extended. The orientation of each stem relative to stem II is given in Table 3. Stems I and II are nearly coaxial, forming an interhelical angle of 153°, while stem III is close to perpendicular to these stems, forming angles of 77° and 100° with stems I and II, respectively. The helical axes of the three stems in the hammerhead are not coplanar but are arranged in a slight pyramidal shape. Previous studies indicated that the precision of the global structure of a multidomain macromolecule is only slightly influenced by the experimental errors for the RDCs (*24*, *25*, *62*). Test calculations with simulated dipolar couplings which

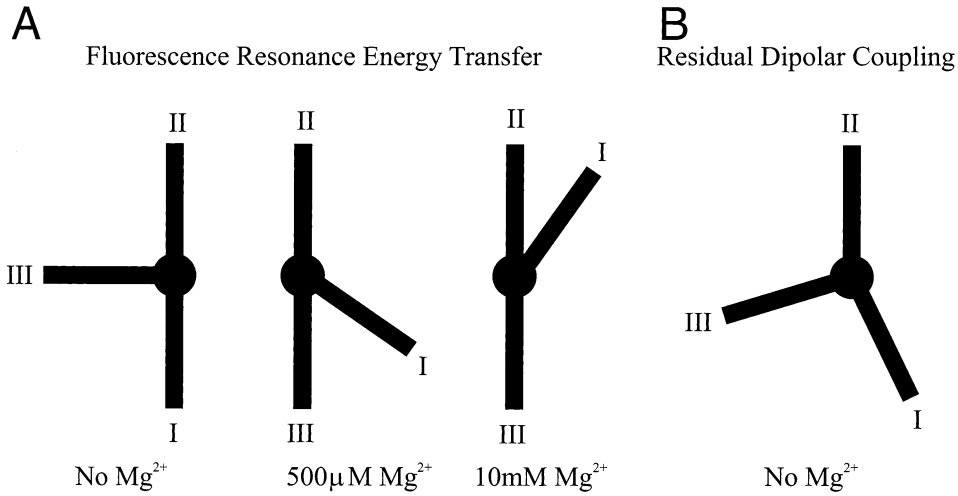

FIGURE 6: (A) Schematic of global conformation of the hammerhead ribozyme as a function of the Mg^{2+} concentration derived from FRET studies (*19, 64*). (B) Schematic of global conformation of the hammerhead ribozyme in solution derived from dipolar coupling data in the absence of Mg^{2+}.

mimicked the experimental data on the hammerhead and incorporated random errors for the dipolar couplings show that only a 1−3° uncertainty for the angles in Table 3 is caused by uncertainty in the dipolar couplings (data not shown). However, other calculations show a larger (2−9°) uncertainty in the relative orientation of the stems arising from differences in local structure in the three crystal structures. From these simulations, we estimate an uncertainty of <10° in our determination of the interhelical angles in the hammerhead.

When a molecule aligns by a steric-type mechanism, it is predicted to have similar alignment and diffusion tensors (the latter is well approximated by the inertia tensor), where the properties of both tensors are dictated by the overall shape of the molecule (*63*). An important confirmation of our global structural model for the hammerhead ribozyme (Figure 5A) is that the principal axes of the alignment tensor of the molecule are nearly parallel to the principal axes of the inertia tensor calculated from the atomic coordinates of the model, as seen in Figure 1S of the Supporting Information. The similar properties for the alignment tensor and the diffusion tensor provide additional support for the global conformational model of the hammerhead determined here. It should be pointed out, however, that the exact conformation of the core could not be determined on the basis of the limited NMR data here. Since the RDCs contain only orientational information on the stems, there may be some additional minor translational variations for the stems caused by the structural variation of the conserved core in the hammerhead.

The NMR global conformation in solution is very different from that observed in the crystal (Figure 5A,B) (*9*). Comparison of the measured dipolar couplings in solution with the predicted dipolar couplings for three X-ray structures (Figure 4) unambiguously demonstrates that the solution conformation in the absence of Mg^{2+} is different from the X-ray structures (which are obtained at high ionic strength or in Mg^{2+}). However, the global conformation of the hammerhead ribozyme determined here (Figure 5A) is consistent with the results of the gel electrophoresis and FRET studies of the hammerhead in the absence of divalent metal ions (*19, 64*). Analysis of the electrophoretic mobilities of hammerhead species with two elongated stems (*20, 64*) suggested that in the absence of metal ions the hammerhead adopts a conformation where the helical stems are connected by a rather unstructured extended core. In this conformation, stems I and II subtend a large angle, similar to the collinear orientation of these two stems found by transient electric birefringence (*20*), whereas smaller angles are observed between stems I−III and II−III. This observation is confirmed by FRET studies which also suggest that stem III is roughly perpendicular to both stems I and II (*19*).

The global structure of the hammerhead determined here was obtained in the presence of 100 mM Na^+ ions. The structure derived from the dipolar coupling data has a large angle (153°) between stems I and II and a smaller angle (100°) between stems II and III, and the smallest angle is between stems I and III (77°) (see Figure 5A). This is qualitatively similar to the interstem angles as predicted from the gel mobility patterns and FRET efficiencies (*19, 64*). Thus, the dipolar coupling NMR data reinforce previous solution studies (*19, 64*) demonstrating that concentrations of 50−100 mM Na^+ do not induce the folded conformation adopted by the hammerhead in the presence of Mg^{2+}. However, there are some differences between the NMR and FRET results. FRET efficiencies measured at low ionic strength suggest approximately equal angles subtended by stems I and III, and stems II and III, as well as an unfolded core with domain 2 not yet formed. In contrast, the NOE data obtained here in the presence of 100 mM Na^+ ions show base-pairing of G8:A13 and A9:G12 in domain 2, indicating that the hammerhead core has a partially folded structure under this condition. This partial folding of domain 2 brings stem I closer to stem III, forming an acute angle of 77°. Lilley and co-workers have proposed a two-step folding mechanism for the hammerhead, with a low Mg^{2+} transition involving formation of domain 2, coaxial stacking of stems II and III, and stem I forming an acute angle with stem III (see Figure 6) (*19*). There is a second Mg^{2+} transition involving folding of domain 1, and above 10 mM Mg^{2+}, the gel mobility (*18*), TEB (*65*), and FRET experiments (*19, 66*), are all consistent with the X-ray structures (*9, 10*), where stem II coaxially stacks with stem III but stem I forms an acute angle with stem II (Figures 5B and 6).

CONCLUSIONS

We have determined the global solution structure of the hammerhead ribozyme from NMR residual dipolar coupling data under low salt conditions in the absence of Mg^{2+} ions. This report together with our previous work on tRNA (*25*) clearly demonstrates that the RDCs measured for the helical stems of an RNA molecule provide important long-range structural information that can be used to obtain the global solution conformation of RNAs from a relatively small set of experimental data. Careful analysis of the alignment tensor components and the related generalized order parameters for each domain is necessary to confirm the applicability of the method for global structure determination to the macromolecular system of interest. The RDC data also provide information about the global dynamics of the molecule and its interaction with the orienting medium.

The global solution structure of the hammerhead ribozyme presented here is very different from the crystal structures that are at high ionic strength or in Mg^{2+}. The structure is in good agreement with the qualitative results for the hammerhead conformation in low salt solution obtained from FRET, gel mobility, and TEB experiments (*18*, *19*, *65*, *66*). The hammerhead has a slightly pyramid-shaped conformation where stems I and II form an angle of 153° and are connected by a stretch of nucleotides in the conserved core that adopts a rather extended conformation. Stem III is almost perpendicular to the other two stems. The RDC data argue against the presence of internal motion involving significant conformational rearrangement of the stems, illustrating that these NMR data provide qualitative information on the domain dynamics of molecules in solution. We are currently extending these NMR studies to test for changes in the global structure and dynamics of the hammerhead as a function of Mg^{2+}.

ACKNOWLEDGMENT

We thank Dr. Paul Hanson for the purified Pf1 phage, Arlene Hangar for synthesis of several of the labeled hammerhead ribozymes, and Drs. Scott McCallum, Hongjun Zhou, and Fiona Jucker for valuable discussions.

SUPPORTING INFORMATION AVAILABLE

Tables S1−S4 give the restraints used in the molecular dynamics calculations. Tables S5 and S6 give the alignment tensor information for reorientation of helical stems relative to fixed stem I and stem II, respectively. Table S7 gives the average pairwise RMSD for the structural ensembles of the hammerhead using the subset and full set of restraints. Figure S1 shows the orientation of the principal axes of the inertia tensor and the alignment tensor for the hammerhead. This material is available free of charge via the Internet at http://pubs.acs.org.

REFERENCES

1. Symons, R. H. (1992) *Annu. Rev. Biochem. 61*, 641−671.
2. Lilley, D. M. J. (1999) *Curr. Opin. Struct. Biol. 9*, 330−338.
3. Eckstein, F., and Bramlage, B. (1999) *Biopolymers 52*, 147−154.
4. Uhlenbeck, O. C. (1987) *Nature 328*, 596−600.
5. Murray, J. B., Seyhan, A. A., Walter, N. G., Burke, J. M., and Scott, W. G. (1998) *Chem. Biol. 5*, 587−595.
6. O'Rear, J. L., Wang, S. L., Feig, A. L., Beigelman, L., Uhlenbeck, O. C., and Herschlag, D. (2001) *RNA 7*, 537−545.
7. Wedekind, J. E., and McKay, D. B. (1998) *Annu. Rev. Biophys. Bioeng. 27*, 475−502.
8. Scott, W. G. (1999) *Q. Rev. Biophys. 32*, 241−284.
9. Pley, H. W., Flaherty, K. M., and McKay, D. B. (1994) *Nature 372*, 68−74.
10. Scott, W. G., Finch, J. T., and Klug, A. (1995) *Cell 81*, 991−1002.
11. Scott, W. G., Murray, J. B., Arnold, J. R. P., Stoddard, B. L., and Klug, A. (1996) *Science 274*, 2065−2069.
12. McKay, D. B. (1996) *RNA 2*, 395−403.
13. Birikh, K. R., Heaton, P. A., and Eckstein, F. (1997) *Eur. J. Biochem. 245*, 1−16.
14. Murray, J. B., Terwey, D. P., Maloney, L., Karpeisky, A., Usman, N., Beigelman, L., and Scott, W. G. (1998) *Cell 92*, 665−673.
15. Torres, R. A., and Bruice, T. C. (2000) *J. Am. Chem. Soc. 122*, 781−791.
16. Peracchi, A., Beigelman, L., Scott, E. C., Uhlenbeck, O. C., and Herschlag, D. (1997) *J. Biol. Chem. 272*, 26822−26826.
17. Murray, J. B., and Scott, W. G. (2000) *J. Mol. Biol. 296*, 33−41.
18. Bassi, G. S., Murchie, A. I., and Lilley, D. M. (1996) *RNA 2*, 756−768.
19. Bassi, G. S., Murchie, A. I. H., Walter, F., Clegg, R. M., and Lilley, D. M. J. (1997) *EMBO J. 16*, 7481−7489.
20. Gast, F. U., Amiri, K. M. A., and Hagerman, P. J. (1994) *Biochemistry 33*, 1788−1796.
21. Tjandra, N., and Bax, A. (1997) *Science 278*, 1111−1114.
22. Bax, A., Kontaxis, G., and Tjandra, N. (2001) *Methods Enzymol. 339*, 127−174.
23. Fischer, M. W., Losonczi, J. A., Weaver, J. L., and Prestegard, J. H. (1999) *Biochemistry 38*, 9013−9022.
24. Skrynnikov, N. R., Goto, N. K., Yang, D., Choy, W., Tolman, J. R., Mueller, G. A., and Kay, L. E. (2000) *J. Mol. Biol. 295*, 1265−1273.
25. Mollova, E. T., Hansen, M. R., and Pardi, A. (2000) *J. Am. Chem. Soc. 122*, 11561−11562.
26. Tsui, V., Zhu, L., Huang, T. H., Wright, P. E., and Case, D. A. (2000) *J. Biomol. NMR 16*, 9−21.
27. Bewley, C. A., and Clore, G. M. (2000) *J. Am. Chem. Soc. 122*, 6009−6016.
28. Sibille, N., Pardi, A., Simorre, J. P., and Blackledge, M. (2001) *J. Am. Chem. Soc. 123*, 12135−12146.
29. Nikonowicz, E. P., Sirr, A., Legault, P., Jucker, F. M., Baer, L. M., and Pardi, A. (1992) *Nucleic Acids Res. 20*, 4507−4513.
30. Shields, T. P., Mollova, E., Marie, L. S., Hansen, M. R., and Pardi, A. (1999) *RNA 5*, 1259−1267.
31. Pardi, A. (1995) *Methods Enzymol. 261*, 350−380.
32. Simorre, J. P., Zimmermann, G. R., Pardi, A., Farmer, B. T., II, and Mueller, L. (1995) *J. Biomol. NMR 6*, 427−432.
33. Simorre, J. P., Zimmermann, G. R., Mueller, L., and Pardi, A. (1996) *J. Am. Chem. Soc. 118*, 5316−5317.
34. Simorre, J. P., Zimmermann, G. R., Mueller, L., and Pardi, A. (1996) *J. Biomol. NMR 7*, 153−156.
35. Hansen, M. R., Mueller, L., and Pardi, A. (1998) *Nat. Struct. Biol. 5*, 1065−1074.
36. Hansen, M. R., Hanson, P., and Pardi, A. (2000) *Methods Enzymol. 317*, 220−240.
37. Zweckstetter, M., and Bax, A. (2001) *J. Biomol. NMR 20*, 365−377.
38. Cordier, F., Dingley, A. J., and Grzesiek, S. (1999) *J. Biomol. NMR 13*, 175−180.
39. Brutscher, B., Boisbouvier, J., Pardi, A., Marion, D., and Simorre, J. P. (1998) *J. Am. Chem. Soc. 120*, 11845−11851.
40. Weigelt, J. (1998) *J. Am. Chem. Soc. 120*, 10778−10779.
41. Tjandra, N., and Bax, A. (1997) *J. Magn. Reson. 124*, 512−515.
42. Mueller, U., Schubel, H., Sprinzl, M., and Heinemann, U. (1999) *RNA 5*, 670−677.
43. Lavery, R., and Sklenar, H. (1989) *J. Biomol. Struct. Dyn. 6*, 655−667.
44. Brünger, A. T. (1992) *X-PLOR 3.1: A System for X-ray Crystallography and NMR*, Yale University Press, New Haven.
45. Schwalbe, H., Marino, J. P., King, G. C., Wechselberger, R., Bermel, W., and Griesinger, C. (1994) *J. Biomol. NMR 4*, 631−644.
46. Cornell, W. D., Cieplak, P., Bayly, C. I., Gould, I. R., Merz, K. M., Jr., Ferguson, D. N., Spellmeyer, D. C., Fox, T., Caldwell, J. W., and Kollman, P. A. (1996) *J. Am. Chem. Soc. 118*, 2309−2309.
47. Hoogstraten, C. G., Legault, P., and Pardi, A. (1998) *J. Mol. Biol. 284*, 337−350.

48. Vermeulen, A., Zhou, H. J., and Pardi, A. (2000) *J. Am. Chem. Soc. 122*, 9638−9647.
49. Prestegard, J. H., Al-Hashimi, H. M., and Tolman, J. R. (2000) *Q. Rev. Biophys. 33*, 371−424.
50. Tjandra, N., Tate, S., Ono, A., Kainosho, M., and Bax, A. (2000) *J. Am. Chem. Soc. 122*, 6190−6200.
51. Zhou, H., Vermeulen, A., Jucker, F. M., and Pardi, A. (2001) *Biopolymers 52*, 168−180.
52. Bruschweiler, R., Liao, X. B., and Wright, P. E. (1995) *Science 268*, 886−889.
53. Ramirez, B. E., and Bax, A. (1998) *J. Am. Chem. Soc. 120*, 9106−9107.
54. Al-Hashimi, H. M., Valafar, H., Terrell, M., Zartler, E. R., Eidsness, M. K., and Prestegard, J. H. (2000) *J. Magn. Reson. 143*, 402−406.
55. Ruckert, M., and Otting, G. (2000) *J. Am. Chem. Soc. 122*, 7793−7797.
56. Tolman, J. R., Al-Hashimi, H. M., Kay, L. E., and Prestegard, J. H. (2001) *J. Am. Chem. Soc. 123*, 1416−1424.
57. Gayathri, C., Bothnerby, A. A., Vanzijl, P. C. M., and Maclean, C. (1982) *Chem. Phys. Lett. 87*, 192−196.
58. Menger, M., Eckstein, F., and Porschke, D. (2000) *Nucleic Acids Res. 28*, 4428−4434.
59. Hammann, C., Norman, D. G., and Lilley, D. M. J. (2001) *Proc. Natl. Acad. Sci. U.S.A. 98*, 5503−5508.
60. Blackledge, M. J., Bruschweiler, R., Griesinger, C., Schmidt, J. M., Xu, P., and Ernst, R. R. (1993) *Biochemistry 32*, 10960−10974.
61. Hoogstraten, C. G., Wank, J. R., and Pardi, A. (2000) *Biochemistry 39*, 9951−9958.
62. Goto, N. K., Skrynnikov, N. R., Dahlquist, F. W., and Kay, L. E. (2001) *J. Mol. Biol. 308*, 745−764.
63. Zweckstetter, M., and Bax, A. (2000) *J. Am. Chem. Soc. 122*, 3791−3792.
64. Bassi, G. S., Mollegaard, N. E., Murchie, A. I., von Kitzing, E., and Lilley, D. M. (1995) *Nat. Struct. Biol. 2*, 45−55.
65. Amiri, K. M. A., and Hagerman, P. J. (1994) *Biochemistry 33*, 13172−13177.
66. Tuschl, T., Gohlke, C., Jovin, T. M., Westhof, E., and Eckstein, F. (1994) *Science 266*, 785−789.

BI012167Q